2022 IEEE International Conference on Environment and Electrical Engineering and 2022 IEEE Industrial and Commercial Power Systems Europe (EEEIC / I&CPS Europe) | 978-1-6654-8537-1/22/$31.00 ©2022 IEEE | DOI: 10.1109/EEEIC/ICPSEUROPE54979.2022.9854655

Extended ZVS/ZCS operation of Class-E Inverter for Capacitive Wireless Power Transfer

Luigi Solimene
Dipartimento Energia
G. Ferraris (DENERG)
Politecnico di Torino
Torino, Italy
luigi.solimene@polito.it

Fabio Corti
Dipartimento di Ingegneria
Università di Perugia
Perugia, Italy
fabio.corti@unipg.it

Salvatore Musumeci
Dipartimento Energia
G. Ferraris (DENERG)
Politecnico di Torino
Torino, Italy
salvatore.musumeci@unipg.it

Alberto Reatti
Dipartimento di Ingegneria
dell'informazione (DINFO)
Università di Firenze
Firenze, Italy
alberto.reatti@unifi.it

Carlo Ragusa
Dipartimento Energia
G. Ferraris (DENERG)
Politecnico di Torino
Torino, Italy
carlo.ragusa@polito.it

***Abstract*— In this work, a control strategy for a Class-E inverter for Capacitive Wireless Power Transfer (CWPT) application is proposed. The presented approach allows to stabilize the output power regulating the components values of the resonant tank. A matrix of capacitors is used to adjust the values of capacitances and the magnetic design procedure for the variable inductor is proposed. The obtained performances are evaluated through Plecs simulations and compared with the case without a control strategy.**

Keywords — Capacitive Wireless Power Transfer, Class-E Inverter, Variable Inductor, Magnetics.

I. INTRODUCTION

Wireless Power Transfer (WPT) is assuming a role of primary importance in numerous sectors. This technique is already widely used for electric vehicle battery charging[1]-[3], underwater robotics [4][5], biomedical plants [6][7] and railway applications [8]-[10]. Thanks to the possibility of transferring power through an air gap, it avoids the use of bulky cables making the system simpler and lighter [11]-[12]. Two main group of WPT system can be identified: inductive (IWPT) and capacitive (CWPT) wireless power transfer systems. The IWPT exploit the magnetic induction between two coils, while CWPT systems exploit the electric field generated between two metal plates. While IWPT is already a mature technology and numerous devices are already available in the market, CPWT systems are still a relatively new technology. Since in a CWPT the power is transferred using cheap metallic plates and does not require high-cost magnetic cores and litz wires, it represents a cheaper solution with respect to IWPT [13]. In addition, since the power is transferred through an electric field between the metal plates, this technology is characterized by lower electromagnetic emissions with respect to IWPT systems where the magnetic field between coils tends to propagate in any direction [14].

One of the most critical wireless power transfer systems problems is the misalignment between plates and the variable operating conditions. Since resonance is created to reduce the reactive power circulating in the power converter and maximize the active power transmission, a small variation of couplings or load variations can significantly affect the power converter's output power and efficiency [15]-[17]. Most of the efforts available in literature are focused on the analysis of innovative circuit topologies able to obtain high efficiency under a particular operating condition [18]. Several different topologies have been used for CWPT. Usually, the most used topology for high power applications to impress a high-frequency voltage to the resonant tank is the full-bridge inverter [19][20][21]. Other single switch topologies have been used for CWPT, such as Buck-Boost, Cuk, Zeta and Sepic [22]. In [23], a Buck-Boost converter for CWPT has been proposed reaching up to 1kW output power. The Class-E inverter represents a suitable topology for CWPT. This topology is made up by a single switch. If the system is adequately designed, the power MOSFET can operate under Zero Voltage Switching (ZVS) and Zero Current Switching (ZCS), leading to low switching power losses and high conversion efficiency. This topology has been widely used for CWPT [24][25][26]. An extensive overview of Class-E inverter topologies for CWPT is shown in [27]. These topologies differ by the resonant compensation used to create resonance and maximize the power transmission. As shown in [27], the LC compensation represents a good compromise between simplicity and performance. However, the output power and the conversion efficiency are highly affected by coupling misalignment. For this reason, in this paper, a control strategy able to maintain high performance under coupling variations is presented.

Several efforts have been made to propose control strategies to maintain optimum operation under variable operating conditions. For example, in [28], two control strategies able to maintain the Class-E inverter operating in ZCS/ZVS under load resistance variation are presented. These approaches consist of changing a resonant tank component value and the operating frequency. Unfortunately, operating with variable frequency does not allow for the optimization of the filter components and usually produces electromagnetic emission issues. For this reason, techniques which operates are constant frequency are preferred for this application.

In this paper, a control strategy able to maintain the power MOSFET operating at ZVS/ZCS conditions under capacitive coupling conditions is proposed. The technique adapts the resonant inductor L_r, the resonant capacitor C_r and the shunt capacitor C_{shunt} according to the operating condition. While

the variable capacitances can be easily realized through matrix of capacitors, the realization of variable inductance is more challenging. For this reason, particular attention is placed on the magnetic design of the variable inductor.

The article is structured as follows. In Section II, the Class-E inverter for the CWPT application is presented. The design procedure is shown. In Section III, the inductor design is presented. In Section IV the simulation results using Plecs are shown, while in Section V the conclusions are discussed.

II. Capacitive WPT Class-E Inverter

The Class-E inverter for CWPT is shown in Fig. 1. The DC input voltage V_i is used to supply the circuit. The classic Class-E inverter topology consists of a choke inductor L_f, a power MOSFET S, a shunt capacitor C_{shunt}, a resonant inductor L_r and a resonant capacitor C_r. The ZVS/ZCS condition is reached when the equivalent impedance Z_R is purely resistive. The equivalent six capacitors shown in [29] are used to model the electrical coupling between the four plates. It is assumed that the cross-coupling capacitances between the plates can be neglected. Thus, the coupling between plates can be simplified with a simple capacitance C_M. Then, an LC compensation is used, represented by the capacitors C_1, C_2 and the inductors L_1 and L_2. The equivalent impedance of the CWPT is Z_{eq}. To obtain a purely resistive impedance $Z_{RL}=R_{eq}$, an external impedance X_{ext} is added to cancel the reactive part, such that $X_{eq}=-X_{ext}$.

A. Design Procedure

Studying the circuit shown in Fig. 1(a), the real and imaginary part of the equivalent impedance $Z_{eq} = R_{eq}+jX_{eq}$ can be calculated

$$R_{eq}=\frac{\beta^2(2R+R_L)+C(R+R_L)(C+2C_M)\left[C^2\omega^2\delta+2\omega^2L(C+C_M)+2C_MC\omega^2\delta-1\right]}{\alpha+\beta} \tag{1}$$

$$X_{eq}=\frac{\beta\left[\left(C^2\omega^2\delta+2\omega^2L(C+C_M)+2C_MC\omega^2\delta-1\right)-\omega^2C(R+R_L)(C+2C_M)(2R+R_L)\right]}{\omega\left(\alpha+\beta^2\right)} \tag{2}$$

where

$$\alpha=\beta+C^2\omega^2\left(R+RL\right)^2\left(C+2C_M\right)^2 \tag{3}$$

$$\beta=-LC^2\omega^2-2C_MLC\omega^2+C+C_M \tag{4}$$

$$\delta=-L_2\omega^2+R_2+R_LR \tag{5}$$

The capacitors C_1 and C_2 are designed to resonate with the inductances L_1 and L_2

$$C_1=\frac{1}{\omega_0^2L_1},\ C_2=\frac{1}{\omega_0^2L_2} \tag{6}$$

The plates are assumed to be identical, thus symmetrical stricture can be assumed $R_1=R_2=R$, $L_1=L_2=L$ and $C_1=C_2=C$.
To reduce the reactive power, the reactive part of the equivalent impedance X_{eq} must be cancelled by adding an external reactance X_{ext} in series, leading to $X_{ext} = - X_{eq}$.
Under this condition, a purely resistive equivalent impedance is obtained $Z_{eq} = R_{eq}$ at $C_M = C_M^{opt}$. Depending on the coupling capacitance C_M, a positive or negative imaginary part X_{eq} can occur, as shown in Fig. 1(b).

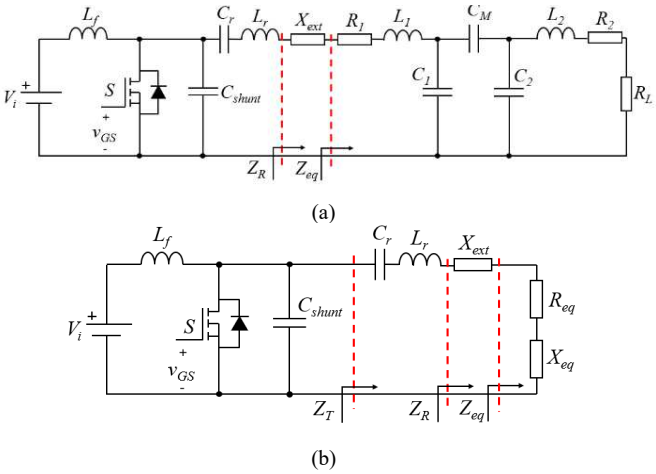

Fig. 1. Class-E inverter topology for CWPT. (a) Circuit with capacitive wireless power system. (b) Equivalent circuit.

If $X_{eq}<0$, an external inductor must be placed as

$$L_{ext}=-\frac{1}{\omega X_{eq}}=\frac{1}{\omega^2C_{eq}} \tag{7}$$

If $X_{eq}>0$, an external capacitance must be connected as

$$C_{ext}=\frac{1}{\omega X_{eq}}=\frac{1}{\omega^2L_{eq}} \tag{8}$$

Assuming that the load resistance R_L, the operating frequency ω_0, and the output power P_o values are known as design specifications, the expressions for the components needed to reach the ZVS condition at $C_M=C_M^{opt}$ are given by

$$V_i=\sqrt{\frac{\pi^2+4}{8}P_oR_{eq}} \tag{9}$$

$$C_{shunt}=\frac{8}{\pi\left(\pi^2+4\right)}\frac{1}{\omega R_{eq}} \tag{10}$$

$$L_r=\frac{Q_LR_{eq}}{\omega} \tag{11}$$

$$C_r=\frac{1}{\omega R_{eq}\left(Q_L-\frac{\pi\left(\pi^2-4\right)}{16}\right)} \tag{12}$$

$$L_f=\frac{7R_{eq}}{f} \tag{13}$$

The constraints of the system analysed in this paper are shown in Table I. Using equations (9)-(13), the values of the components shown in Table II can be obtained.

TABLE I. CWPT System Characteristics

Parameter	Value
Output Power P_o	50 W
Load Resistance R_L	5 Ω
Operating Frequency f_s	200 kHz
Quality Factor Q_L	10
Coupling Capacitance C_M^{opt}	200 pF
Inductances Parasitic Resistances ESR_{Lf1}, ESR_{Lf2}, ESR_{L1}, ESR_{L2}	100 mΩ
Primary and Secondary Inductance L_1, L_2	100 µH

TABLE II. RESONANT COMPENSATIONS PARAMETERS

Parameter	Value
External Inductor C_1, C_2	6.3 nF
External Capacitance C_{ext}	327.3 nF
Resonant Inductances L_r	14.9 µH
Resonant Capacitances C_r	48 nF

The impedance $Z_R=R_R+jX_R$ under coupling capacitance C_M variation is evaluated as shown in Fig. 2(a). As can be seen, both the real and imaginary parts increase as the coupling increases. In particular, the imaginary part X_R is equal to zero at the optimum coupling capacitance C_M = 200 pF. Then, it acts as an inductor $L_r=X_r/\omega$ for couplings $C_M > C_M^{opt}$, while it acts as a capacitance $C_r=1/(\omega X_r)$ when the coupling is $C_M < C_M^{opt}$. This reactance is anyway negligible. In fact, as shown in Fig. 2(a), the maximum value is approximately $X_r^{max}=0.1$ Ω, leading to an equivalent inductance L_R=79.5 nH. Since the resonant inductance L_r=14.9 µH and it is connected in series, its contribution can be neglected $L_R<<L_r$. On the other hand, the minimum reactance value is approximately X_r^{min}= - 0.25 Ω, leading to an equivalent capacitance C_R = 3.2 µF. Since the resonant capacitor C_r = 48 nF is connected in series, its contribution can be neglected $C_R>>C_r$. For this reason, the main effect on the Class-E inverter is related to the variation of the resistive part of Z_R.

As shown in (9), (10) and (11), the values of capacitances C_r and C_{shunt} and inductance L_r required to maintain the Class-E inverter operating at ZVS/ZCS depend on the equivalent load resistance R_R. For this reason, this paper proposes a control strategy to maintain the power converter operating in ZCS/ZVS in a wide range of coupling capacitance variations. In Fig. 2(b), the required value of inductance for different coupling capacitance is shown. The following section describes the procedure used to design the variable inductor.

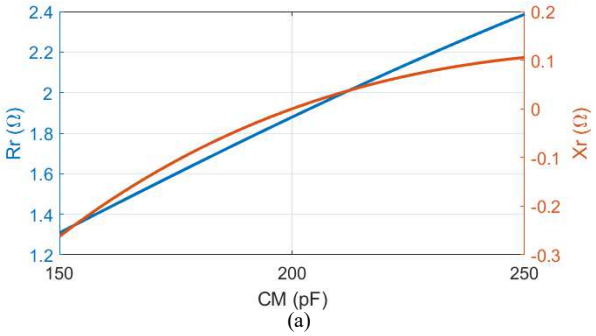

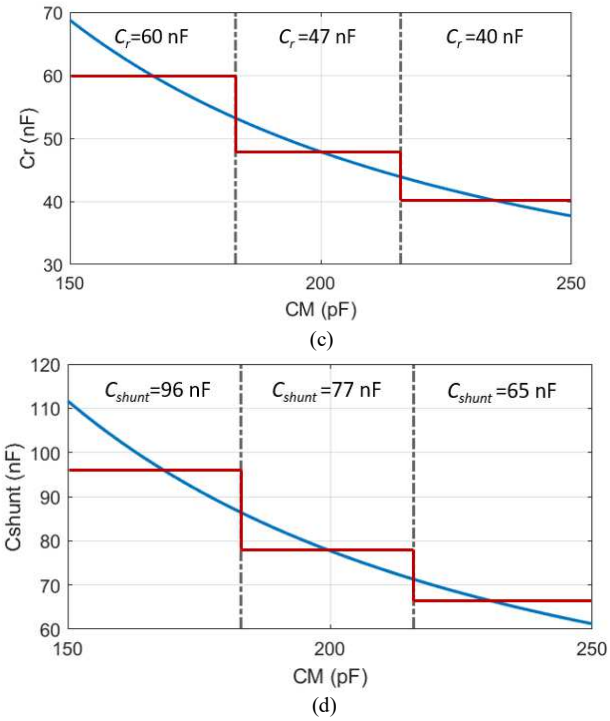

Fig. 2. Effect of coupling coefficient variations. (a) Resistive and reactive part of the impedance Z_R. (b) Resonant inductance L_r required for different coupling. (c) Required resonant capacitance C_r. (d) Required shunt capacitance C_{shunt}.

In Fig. 2(c), the variation of C_{shunt} is presented. A variable capacitance between 60nF < C_{shunt} < 110nF is required. A matrix of capacitance represents the simplest solution to solve this issue. This approach has been already widely used in a Class-E inverter for WPT applications. The range of variations of C_M is divided into three parts, and depending on the operating condition, a particular capacitor is selected, as shown in Fig. 2(c). Finally, the same approach can be used to realize the variable capacitance C_r in the range 37nF < C_r < 69nF, as shown in Fig. 2(d).

III. VARIABLE INDUCTOR DESIGN

Different approaches have been proposed to create variable inductors. The simpler solution to obtain a variable inductor consists of switches that select different inductors values. However, this solution is expensive and bulky since several components are required. In [30], a variable inductance is obtained, varying the air gap by inclined or stagger aperture structure mode. However, its manufacturing is not simple, resulting in higher costs. For this reason, the most used approaches consist of changing the magnetic permeability of the material using an additional magnetic polarization flux in addition to the main inductor magnetic flux, shifting the magnetic induction [31]. This approach has been widely used to control LLC converter [32]- [37].

The principle of a controlled variable inductor is the variation of the differential permeability of a ferromagnetic material, defined as

$$\mu_d = \frac{1}{\mu_0}\frac{dB}{dH}. \quad (14)$$

The variation of the applied magnetic field strength leads the magnetic material to operate in the different regions of the magnetization curve, from a linear region, where the

differential permeability shows a near-constant profile, to a roll-off region, in which the permeability rapidly decreases, finally to a saturation region, where the minimum value of the differential permeability is obtained, and the material is fully saturated [36]. Fig. 3 represents the magnetization curve and the differential permeability profile of a Mn-Zn ferrite, highlighting the three different operating regions.

A practical topology of a controlled variable inductor is composed of a double E core with the main winding placed on the central leg and connected to the resonant tank of the CWPT system and two auxiliary winding placed on the outer legs of the core [37]. By controlling the direct current value in the auxiliary windings, the applied magnetomotive force in the core is varied, and thus the applied magnetic field strength in the magnetic material is controlled. The auxiliary windings are connected in series with opposite polarity to force the DC magnetic flux path only in the outer legs of the double E core. Instead, the central leg operates in the linear region of the magnetization curve and is designed to assure the component exhibits a linear behaviour when excited with the AC magnetomotive force swing.

To this end, a concentrated air gap is adopted in the central leg of the selected core. Fig. 4(a) represents the arrangement of the considered core geometry. The equivalent reluctance model depicted in Fig. 4(b) can be used to compute the differential inductance profile referred to the main winding [38].

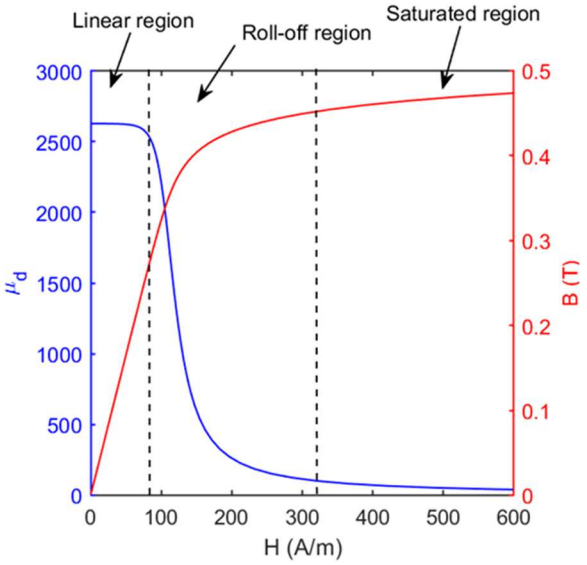

Fig. 3. Magnetization curve of a Mn-Zn ferrite. The red line represents the B-H curve and the blue line represents the related differential permeability profile. The three different operating regions of soft magnetic material are highlighted.

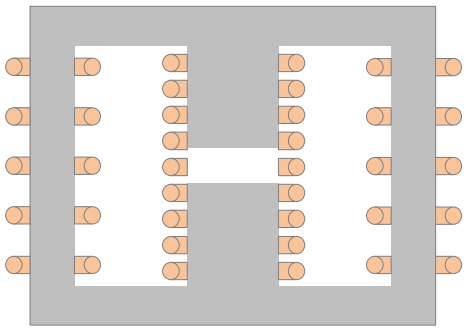

(a)

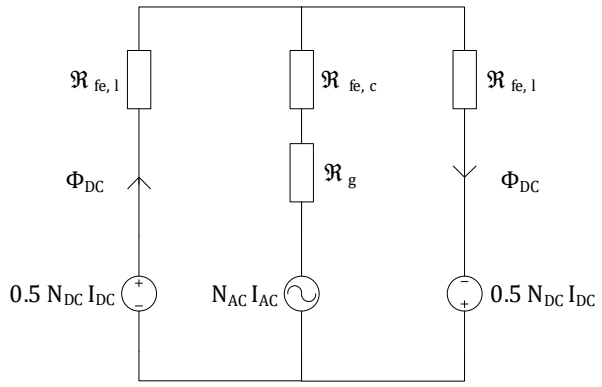

(b)

Fig. 4. Description of the core and winding configuration for the variable inductor design. (a) Detail of the double E core gapped configuration. (b) Equivalent reluctance circuit.

The air gap reluctance and the ferromagnetic path reluctance can be described as constant terms by

$$\Re_{fe,c} = \frac{l_{fe,c}}{\mu_0 \mu_{fe,in} S_{fe,c}}, \tag{15}$$

$$\Re_g = \frac{l_g}{\mu_0 S_g}, \tag{16}$$

while the reluctance of the outer legs ferromagnetic path can be described as a function of the magnetomotive force applied by the auxiliary windings:

$$\Re_{fe,l}(N_{DC} I_{DC}) = \frac{l_{fe,l}}{\mu_0 \mu_{fe,d}(N_{DC} I_{DC}) S_{fe,c}}. \tag{17}$$

The equivalent reluctance referred to main winding is defined as

$$\Re_{eq}(N_{DC} I_{DC}) = \Re_{fe,c} + \Re_g + 0.5 \cdot \Re_{fe,l}(N_{DC} I_{DC}), \tag{18}$$

and thus, the differential inductance can be computed as

$$L(N_{DC} I_{DC}) = \frac{N_{AC}^2}{\Re_{eq}(N_{DC} I_{DC})} \tag{19}$$

To obtain a variable inductance profile suitable for the specification of the designed CWPT system, an N87 double E 25/13/7 core is selected, with 0.5 mm gap on the central leg, 12 turns on the main winding and 10 turns of the auxiliary windings, equally split on the outer legs. The supply of the auxiliary windings can be realized with a synchronous buck converter, and the current value to control the differential inductance value is obtained through a PI regulator.

IV. Simulation Results

The obtained output power and transmission efficiency results are shown in Fig. 5(a) and (b), respectively. The blue dots are the simulation measurements using Plecs for the system employing the proposed approach with variable components. As shown in Fig. 5(a), the proposed method allows maintaining the output voltage close to the desired value P_o=50W in the whole operating conditions. On the other hand, when the components are maintained fixed, the output power is close to the target value P_o=50W only when the system operates close to the nominal condition C_M^{opt}=200pF. The output power increases for lower couplings and decreases for higher couplings. The efficiency is analyzed in Fig. 5(b). The proposed control technique allows higher DC-AC conversion efficiency over the whole

capacitive coupling range since the system constantly operates in ZVS/ZCS. As expected, the system with fixed components obtains comparable efficiency close to the nominal condition C_M^{opt}=200pF.

V. Conclusions

In this paper, a control strategy for a Class-E inverter for CWPT application is presented. The proposed approach allows to maintain a constant output power over a wide coupling capacitance variation range. High efficiency is obtained since the ZVS/ZCS condition is maintained in the coupling variation range. The benefits with respect to the case of fixed components are shown, showing a comparison in terms of efficiency and output power.

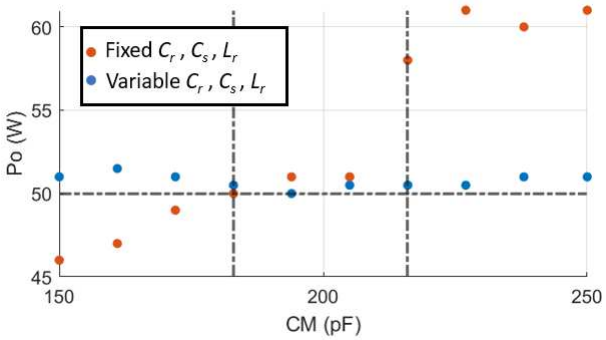

(a)

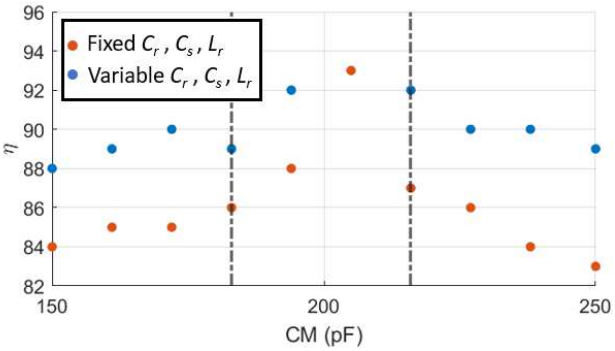

(b)

Fig. 5. Obtained simulation results. Red points represent the measurements of the system with fixed values. Blue points represent the measurements with the proposed control strategy. (a) Output power. (b) Conversion efficiency.

References

[1] P. Machura, V. De Santis and Q. Li, "Driving Range of Electric Vehicles Charged by Wireless Power Transfer," in *IEEE Transactions on Vehicular Technology*, vol. 69, no. 6, pp. 5968-5982, June 2020, doi: 10.1109/TVT.2020.2984386.

[2] A. Reatti *et al*., "Application of induction power recharge to garbage collection service," *2017 IEEE 3rd International Forum on Research and Technologies for Society and Industry (RTSI)*, 2017, pp. 1-5, doi: 10.1109/RTSI.2017.8065961.

[3] A. Ahmad, M. S. Alam and R. Chabaan, "A Comprehensive Review of Wireless Charging Technologies for Electric Vehicles," in *IEEE Transactions on Transportation Electrification*, vol. 4, no. 1, pp. 38-63, March 2018, doi: 10.1109/TTE.2017.2771619.

[4] Q. Sun *et al*., "A Miniature Robotic Turtle With Target Tracking and Wireless Charging Systems Based on IPMCs," in *IEEE Access*, vol. 8, pp. 187156-187164, 2020, doi: 10.1109/ACCESS.2020.3026333.

[5] B. Allotta et al., "Wireless power recharge for underwater robotics," *2017 IEEE International Conference on Environment and Electrical Engineering and 2017 IEEE Industrial and Commercial Power Systems Europe (EEEIC / I&CPS Europe)*, 2017, pp. 1-6, doi: 10.1109/EEEIC.2017.7977478.

[6] G. Shao and Y. Guo, "Hybrid Wireless Positioning and Charging With Switched Field Helmholtz Coils for Wireless Capsule Endoscopy," in *IEEE Transactions on Microwave Theory and Techniques*, vol. 68, no. 3, pp. 904-913, March 2020, doi: 10.1109/TMTT.2019.2959762.

[7] A. I. Mahmood, S. K. Gharghan, M. A. A. Eldosoky, M. F. Mahmood and A. M. Soliman, "Wireless Power Transfer Based on Spider Web–Coil for Biomedical Implants," in *IEEE Access*, vol. 9, pp. 167674-167686, 2021.

[8] W. Kongwarakom, T. Ratniyomchai and T. Kulworawanichpong, "Analysis and Design of Wireless Charging Lane for Light Rail Transit," *2020 International Conference on Power, Energy and Innovations (ICPEI)*, 2020, pp. 29-32.

[9] L. Pugi, A. Reatti, F. Corti, "Application of Wireless Power Transfer to Railway Parking Functionality: Preliminary Design Considerations with Series-Series and LCC Topologies", Journal of Advanced Transportation, Volume 2018, Article number 8103140, DOI 10.1155/2018/8103140.

[10] F. Turki, V. Staudt and A. Steimel, "Dynamic wireless EV charging fed from railway grid: Grid connection concept," *2015 International Conference on Electrical Systems for Aircraft, Railway, Ship Propulsion and Road Vehicles (ESARS)*, 2015, pp. 1-5.

[11] L. Pugi et al., "Application of modal analysis methods to the design of wireless power transfer systems", Meccanica, Volume 54, Issue 1-2, Pages 321 - 331, 1 January 2019, DOI 10.1007/s11012-018-00940-x.

[12] R. A. Mastromauro et al., "Inductive power transfer: Through a bondgraph analogy, an innovative modal approach," *2017 IEEE International Conference on Environment and Electrical Engineering and 2017 IEEE Industrial and Commercial Power Systems Europe (EEEIC / I&CPS Europe)*, 2017, pp. 1-6, doi: 10.1109/EEEIC.2017.7977737.

[13] J. Dai and D. C. Ludois, "A Survey of Wireless Power Transfer and a Critical Comparison of Inductive and Capacitive Coupling for Small Gap Applications," in *IEEE Transactions on Power Electronics*, vol. 30, no. 11, pp. 6017-6029, Nov. 2015, doi: 10.1109/TPEL.2015.2415253.

[14] R. Zhang, H. Liu, Q. Shao, G. Li, X. Fang and H. Li, "Effects of Wireless Power Transfer on Capacitive Coupling Human Body Communication," in *IEEE/ASME Transactions on Mechatronics*, vol. 20, no. 3, pp. 1440-1447, June 2015, doi: 10.1109/TMECH.2014.2345254.

[15] S. Sinha, A. Kumar, B. Regensburger and K. K. Afridi, "Active Variable Reactance Rectifier—A New Approach to Compensating for Coupling Variations in Wireless Power Transfer Systems," in *IEEE Journal of Emerging and Selected Topics in Power Electronics*, vol. 8, no. 3, pp. 2022-2040, Sept. 2020, doi: 10.1109/JESTPE.2019.2958894.

[16] R. Pagano, S. Abedinpour, A. Raciti, e S. Musumeci, «Efficiency optimization of an integrated wireless power transfer system by a genetic algorithm», in *2016 IEEE Applied Power Electronics Conference and Exposition (APEC)*, mar. 2016, pagg. 3669–3676. doi: 10.1109/APEC.2016.7468398.

[17] R. Pagano, S. Abedinpour, A. Raciti, e S. Musumeci, «Modeling of planar coils for wireless power transfer systems including substrate effects», in *IECON 2016 - 42nd Annual Conference of the IEEE Industrial Electronics Society*, ott. 2016, pagg. 1129–1136. doi: 10.1109/IECON.2016.7793993.

[18] M. Z. Erel, K. C. Bayindir, M. T. Aydemir, S. K. Chaudhary and J. M. Guerrero, "A Comprehensive Review on Wireless Capacitive Power Transfer Technology: Fundamentals and Applications," in *IEEE Access*, vol. 10, pp. 3116-3143, 2022, doi: 10.1109/ACCESS.2021.3139761.

[19] E. Abramov, I. Zeltser and M. M. Peretz, "A network-based approach for modeling resonant capacitive wireless power transfer systems," in *CPSS Transactions on Power Electronics and Applications*, vol. 4, no. 1, pp. 19-29, March 2019, doi: 10.24295/CPSSTPEA.2019.00003.

[20] L. Yang *et al*., "Analysis and design of four-plate capacitive wireless power transfer system for undersea applications," in *CES Transactions on Electrical Machines and Systems*, vol. 5, no. 3, pp. 202-211, Sept. 2021, doi: 10.30941/CESTEMS.2021.00024.

[21] E. Abramov and M. M. Peretz, "Multi-Loop Control for Power Transfer Regulation in Capacitive Wireless Systems by Means of Variable Matching Networks," in *IEEE Journal of Emerging and Selected Topics in Power Electronics*, vol. 8, no. 3, pp. 2095-2110, Sept. 2020.

[22] J. Dai and D. C. Ludois, "Wireless electric vehicle charging via capacitive power transfer through a conformal bumper," *2015 IEEE*

Applied Power Electronics Conference and Exposition (APEC), 2015, pp. 3307-3313, doi: 10.1109/APEC.2015.7104827.

[23] J. Dai and D. C. Ludois, "Single Active Switch Power Electronics for Kilowatt Scale Capacitive Power Transfer," in *IEEE Journal of Emerging and Selected Topics in Power Electronics*, vol. 3, no. 1, pp. 315-323, March 2015, doi: 10.1109/JESTPE.2014.2334621.

[24] H. Ueda and H. Koizumi, "Class-E2 DC-DC Converter With Basic Class-E Inverter and Class-E ZCS Rectifier for Capacitive Power Transfer," in *IEEE Transactions on Circuits and Systems II: Express Briefs*, vol. 67, no. 5, pp. 941-945, May 2020, doi: 10.1109/TCSII.2020.2981131.

[25] F. Corti, A. Reatti, Y-H. Wu, D. Czarkowski, S. Musumeci, "Zero Voltage Switching Condition in Class-E Inverter for Capacitive Wireless Power Transfer Applications", *Energies*, 2021, 14(4):911, https://doi.org/10.3390/en14040911.

[26] L. Huang, A. P. Hu, A. Swain and X. Dai, "Comparison of two high frequency converters for capacitive power transfer," *2014 IEEE Energy Conversion Congress and Exposition (ECCE)*, 2014, pp. 5437-5443, doi: 10.1109/ECCE.2014.6954146.

[27] A. Reatti, S. Musumeci and F. Corti, "Class-E Inverters for Capacitive Wireless Power Transfer in Charger Circuit Applications," *2021 AEIT International Conference on Electrical and Electronic Technologies for Automotive (AEIT AUTOMOTIVE)*, 2021, pp. 1-5, doi: 10.23919/AEITAUTOMOTIVE52815.2021.9662732.

[28] A. Reatti, F. Corti, L. Pugi, M. K. Kazimierczuk, G. Migliazza and E. Lorenzani, "Control Strategies for Class-E Resonant Inverter with Wide Load Variation," *2018 IEEE International Conference on Environment and Electrical Engineering and 2018 IEEE Industrial and Commercial Power Systems Europe (EEEIC / I&CPS Europe)*, 2018, pp. 1-6, doi: 10.1109/EEEIC.2018.8494505.

[29] H. Zhang et al., "A loosely coupled capacitive power transfer system with LC compensation circuit topology", IEEE Energy Conversion Congress and Exposition (ECCE), Milwaukee, WI, USA, 18–22 September 2016; pp. 1–5.

[30] W. H. Wolfle and W. G. Hurley, "Quasi-active power factor correction with a variable inductive filter: theory, design and practice," in *IEEE Transactions on Power Electronics*, vol. 18, no. 1, pp. 248-255, Jan. 2003.

[31] E. A. Bitencourt, M. R. Cosetin, I. G. Vegner and R. N. do Prado, "A ferromagnetic based variable inductor analysis and design methodology," *2015 IEEE 13th Brazilian Power Electronics Conference and 1st Southern Power Electronics Conference (COBEP/SPEC)*, 2015, pp. 1-5, doi: 10.1109/COBEP.2015.7420081.

[32] Y. Wei, D. Woldegiorgis and A. Mantooth, "Variable Resonant and Magnetizing Inductor Control for LLC Resonant Converter," *2020 IEEE 11th International Symposium on Power Electronics for Distributed Generation Systems (PEDG)*, 2020, pp. 149-153, doi: 10.1109/PEDG48541.2020.9244466.

[33] Y. Wei et al., "Comprehensive analysis and design of LLC resonant converter with magnetic control," in *CPSS Transactions on Power Electronics and Applications*, vol. 4, no. 4, pp. 265-275, Dec. 2019, doi: 10.24295/CPSSTPEA.2019.00025.

[34] V. S. Costa, M. S. Perdigão, A. S. Mendes and J. M. Alonso, "Evaluation of a variable-inductor-controlled LLC resonant converter for battery charging applications," *IECON 2016 - 42nd Annual Conference of the IEEE Industrial Electronics Society*, 2016, pp. 5633-5638.

[35] Y. Wei and A. Mantooth, "A Family of LLC Converters with Magnetic Control," *2021 IEEE Applied Power Electronics Conference and Exposition (APEC)*, 2021, pp. 783-789.

[36] C. Ragusa *et al.*, «Computation of current waveform in ferrite power inductors for application in buck-type converters», *Journal of Magnetism and Magnetic Materials*, vol. 502, pag. 166458, mag. 2020, doi: 10.1016/j.jmmm.2020.166458.

[37] W. Ma, X. Xie and S. Jiang, "LLC resonant converter with variable resonant inductor for wide LED dimming range," *2017 IEEE Applied Power Electronics Conference and Exposition (APEC)*, 2017, pp. 2950-2957, doi: 10.1109/APEC.2017.7931116.

[38] S. Musumeci, L. Solimene, and C. Ragusa, «Identification of DC Thermal Steady-State Differential Inductance of Ferrite Power Inductors», *Energies*, vol. 14, n. 13, Art. n. 13, gen. 2021, doi: 10.3390/en14133854.